Environ Geol (2007) 52:293–302
DOI 10.1007/s00254-006-0461-4

ORIGINAL ARTICLE

Drying of salt-contaminated masonry: MRI laboratory monitoring

Teresa Diaz Gonçalves · Leo Pel · José Delgado Rodrigues

Received: 24 May 2006 / Accepted: 7 August 2006 / Published online: 2 December 2006

Abstract Drying of masonry specimens was monitored by means of a two-dimensional (2D) magnetic resonance imaging (MRI) technique. The external surfaces stayed wet for longer if NaCl was present instead of pure water only. This corroborates many practical observations that salts aggravate dampness in masonry. A slower evaporation process and not hygroscopicity was the cause. That suggests that salt-induced dampness may, in general, arise simply from changes in the drying process of masonry materials. That also implies that the height and depth at which crystallization occurs in walls may depend on the relative equilibrium humidity (RHeq) and other properties of salts that influence drying of porous materials. Evaporation rates of free surfaces of pure water and saturated NaCl solution were measured by a gravimetric technique. The results indicate that slow drying of salt-contaminated materials is not due only to the lower RHeq of salt solutions. The effective surface of evaporation is likely to be reduced perhaps due to blocking of pores by salt crystals. Final salt-distribution maps of the specimens show that: (a) salts may affect the inner materials of the masonry, even in evaporation-induced processes that lead crystallization to occur predominantly on the external surface; (b) distinct internal distribution patterns occur if masonry composition varies.

Keywords Magnetic resonance imaging · Drying · Porous materials · Salt decay · Ancient masonry

Electronic supplementary material Supplementary material is available in the online version of this article at http://dx.doi.org/10.1007/s00254-006-0461-4 and is accessible for authorized users.

T. D. Gonçalves (✉) · J. D. Rodrigues
National Laboratory of Civil Engineering,
Lisbon, Portugal
e-mail: teresag@lnec.pt

L. Pel
Department of Applied Physics,
Technical University of Eindhoven,
Eindhoven, The Netherlands

Introduction

Moist surfaces are recurrently found in salt-loaded walls. But, as recently stated by an experienced building pathologist concerning the common case of rising damp, ''... the examination of two closely affiliated phenomena, salt damage and rising damp, leaves us with far less in the way of definitive intervention strategies than we might wish, primarily because our understanding of the phenomena is limited'' (Harris 2001). It is therefore, essential to understand the mechanisms of salt-induced dampness. Hygroscopicity of soluble salts can explain some situations of pathologic dampness. Hygroscopicity refers to the capability of the salts or salt solutions for absorbing moisture from the air. This happens if and when the environmental relative humidity (RH) is higher than the relative equilibrium humidity (RH_{eq}) of the salt or salt solution. In that case, a negative vapour pressure gradient exists between the salt-contaminated surface and the surrounding air. Hence, water vapour diffuses from the environment to the surface. In contrast, when the environmental RH is lower than the RH_{eq} of the salt or salt solution, the vapour pressure gradient is positive. Therefore, water vapour diffuses in the opposite direction, that is to say, from the material to the environment. Hence, the salt-contaminated material dries.

The driving vapour pressure gradient for vapour transport between a wet material and the environment is lower if soluble salts are present because non-volatile solutes depress the RH_{eq} of the solution. This is the reason why porous materials dry more slowly if soluble salts are present. Further, as indicated by theoretical considerations (Hall and Hoff 2002), that reduction of the vapour pressure gradient during drying of porous materials results in advancement of the evaporation front towards the outer surface. This suggests that salt-induced dampness may arise, in general, from changes in the drying process of porous building materials.

It is also mostly during drying that salts spread throughout the masonry. Fundamental research work has been carried out for explaining (Arnold 1989; Steiger et al. 1997) why some salts tend to crystallize at the surface and higher on the wall, while others tend to be deposited at inner depths or closer to the pavement. However, old masonries are heterogeneous systems. They are composed of distinct elements: plaster, bedding mortar and stone or brick. Furthermore, masonry materials may vary from monument to monument. Hence, it is also important to understand drying and deposition processes in more detail.

Drying of salt-contaminated masonry specimens was investigated by means of a magnetic resonance imaging (MRI) technique. The technique provided sequences of two-dimensional (2D) images which map the concentration of liquid water in the specimens at certain moments. Thus, moisture distribution during drying could be monitored. This initial study was restricted to pure water and NaCl contamination, as well as to isothermal drying conditions. Specimens with two alternative types of masonry stone were used. Salt distribution was evaluated at the end of the experiments. Complementarily, evaporation from free surfaces of pure water and saturated NaCl solution was measured by means of a gravimetric technique to help evaluate the influence of this salt on drying.

This paper presents the experimental results and discusses the following main questions: (a) changes in drying of water-filled porous materials induced by the presence of NaCl; (b) influence that masonry composition may have on the final distribution of salt; (c) dampness and salt distribution in real masonry walls contaminated with NaCl or other soluble salts.

Materials and methods

Materials

The drying experiments were performed on two different specimens composed of three building materials representing the three main elements of ancient stone masonry: stone, bedding mortar and plaster (Fig. 1).

Each specimen included a different type of stone: stone D (specimen DL1) and stone M (specimen ML1). Both are very common stones in Portugal so they are expected to be representative of ancient ordinary masonry in this country, normally built from locally available materials (Gonçalves and Rodrigues 2005). The plaster and the bedding mortar were made from the same pure lime mortar (mortar L) in both specimens.

Table 1 and Fig. 2 present the composition and properties of the three materials. It can be seen that: (a) the porosity and, thus, the moisture storage capability of stone M is higher than that of mortar L which is higher than that of stone D; (b) mortar L has less medium-dimension pores (between 0.1 and 0.6 μm) but more coarse pores (larger than 0.6 μm) and significantly more fine pores (smaller than 0.1 μm) than stone D; (c) mortar L has less medium-dimension and coarse pores (between 0.2 and 5 μm) but more fine pores (less than 0.2 μm) and also more coarse pores (larger than 5 μm) than stone M.

Prior to making the specimens, the cut surfaces of the stone elements were sandpapered in order to improve mortar/stone adherence. Next, bedding mortar/stone bases were made by applying mortar L on the stone. The bases were kept in a conditioned room at 20°C and 65% RH for 2 weeks. Afterwards, the plaster was made by applying similar mortar L on these bases. In both cases, the mortar was applied: (a) after pre-wetting the surfaces; (b) with the help of acrylic plaques placed laterally during application and removed around 15 min later. The specimens were maintained in the same conditioned room during the following 5 months before testing. At 2 months of age, they were laterally sealed with epoxy resin.

Drying experiments

Each specimen was tested twice, first with pure water, then with a 3 m NaCl solution. In order to obtain complementary background information, evaporation experiments on free (pure water and NaCl saturated) solutions were also performed. After capillary saturation by total immersion in pure water or in a 3 m NaCl solution, the bottom face of the specimens was sealed with Parafilm M® plastic film.

Magnetic resonance imaging images were collected every 30 min during drying. After the initial MRI image was obtained, air flow at 0% RH (temperature ≈ 18°C) was applied. For pure water, drying was

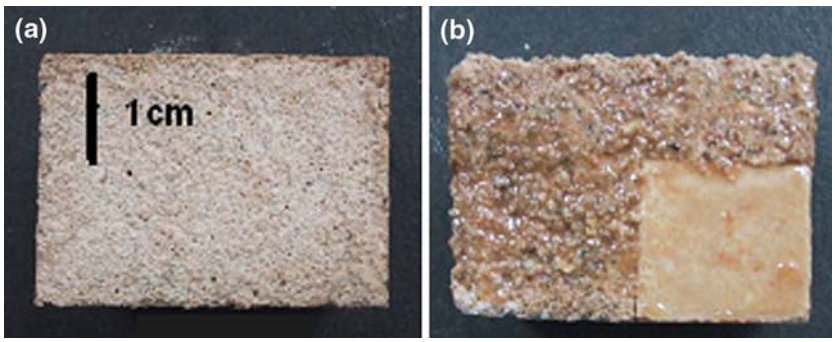

Fig. 1 Pictures of one specimen: **a** top view; **b** lateral view. During drying all faces are sealed except top face (**a**) through which water vapour leaves the porous system

Table 1 Composition, porosity and capillary coefficient of the materials

Material	Volumetric composition/nature	Open porosity[a] (% V)		Capillarity coefficient [kg/(m^2 min$^{1/2}$)]
		By capillary saturation (total immersion)	By total (vacuum) saturation	
Lime mortar L	1:1.5:1.5 (dry hydrated lime:sand from the Tagus river:yellow pit sand from Corroios)	17.6	28.7	1.7
Stone D	Calcitic calcareous stone with fossil fragments (medium porosity)	11.2	15.4	0.5
Stone M	Calcitic calcareous stone (high porosity)	26.6	32.4	1.5

[a] Measured by means of hydrostatic weighting

monitored for 20 h. For the NaCl solution, drying was monitored for 60 h (specimen DL1) and 35 h (specimen ML1).

The evaporation rates of free surfaces of pure water and NaCl saturated solution were measured under environmental conditions of either 20°C-50% RH or 20°C-15% RH. Identical Petri dishes of 77 mm internal diameter and 18 mm depth were used. Two dishes of liquid were tested in either case. Drying took place in a climatic chamber with a low air velocity. Nevertheless, the evaporating areas were possibly smaller than the internal area of the dishes, due to some hindering effect caused by the lateral wall of the dishes. Comparative analysis is, however, possible because an identical height of liquid (13 mm) was used in all cases.

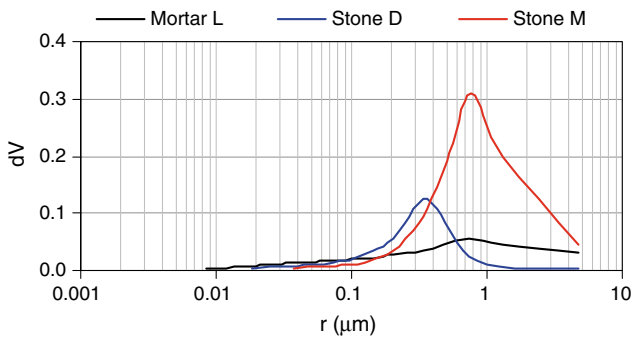

Fig. 2 Pore size distribution (by mercury intrusion porosimetry)

Magnetic resonance imaging

In nuclear magnetic resonance (NMR) techniques, the sample is magnetized by a strong static magnetic field. The nuclei in the sample are afterwards manipulated by radio frequency (RF) pulses at the resonance frequency of these nuclei:

$$\omega = \frac{\gamma \cdot B_0}{2\pi} \quad (1)$$

In this equation, ω is the resonance frequency of the nuclei of interest (MHz), γ their gyromagnetic ratio (MHz/T) and B_0 the strength of the main magnetic field (T). Because of this condition, NMR methods can be made sensitive to one specific type of nuclei. In the present experiment, hydrogen (γ = 42.6 MHz/T), thus, water was detected. In future research, 2D images of the Na^+ ion will also be presented.

The amplitude of the resulting spin-echo signal (S) is proportional to the number of nuclei excited by the RF pulse:

$$S = \rho \cdot e^{-\mathrm{TE}/T_2} \cdot (1 - e^{-\mathrm{TR}/T_1}). \quad (2)$$

In this expression, ρ is the density of the nuclei in the sample, T_1 the spin-lattice relaxation time, TR the repetition time, T_2 the spin-spin relaxation time and TE the echo-time (Westbrook 2002, for instance). In

this technique, a TR of 1.3 s is used. Therefore, TR is long in comparison to T_1 (TR $\geq 4T_1$). Thus, T_1 has no significant influence on signal intensity which is mostly a function of T_2. In building materials, due to the presence of magnetic impurities, T_2 relaxation is short, so a short TE is also preferred. In this case, the TE chosen was 205 μs, the minimum value allowed by the experimental set-up.

A home-built NMR scanner was used (Fig. 3). It incorporates an iron-core electromagnet operating at a field of 0.78 T. The set-up uses two sets of Anderson gradient coils which allow the application of a magnetic gradient G. G is applied at each rotation angle φ (Fig. 4), by suitably changing the values of G_x and G_y:

$$\begin{cases} G_x = G\cos\varphi \\ G_y = G\sin\varphi \end{cases}. \tag{3}$$

A constant total gradient $G = 0.15$ T/m was used, leading to a one-dimensional resolution of around 2 mm.

Radial projections were measured in 32 directions over 180° (Fig. 4). Three averages were taken for each measurement to improve the S/N ratio. These resulted in a total image acquisition time of 30 min.

Afterwards, by using a so-called backward projection program, 2D distributions were calculated.

NMR calibration

The NMR signal may be affected by impurities. Thus, it was necessary to verify if the proportionality constant of Eq. 2 varied among the different materials. For each material, the mean NMR signal value obtained at the very beginning of the pure-water drying experiments was correlated with the capillary saturation moisture content (Table 1). As the correlation values were found to have limited dispersion (Fig. 5), the NMR signal could be assumed as being proportional to the moisture content regardless of the material. Figure 6 shows the colour scale used in the MRI images.

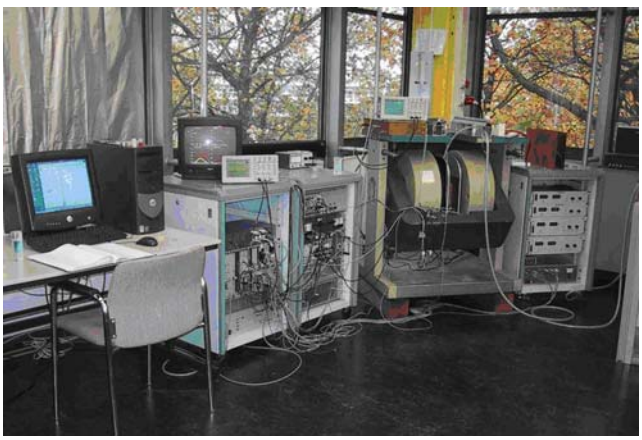

Fig. 3 NMR setup used to measure 2D moisture distribution by means of backwards projection method for building materials

Salt distribution

Final salt distribution in specimens DL1 and ML1 was determined after oven-drying the specimens at 40°C and further removal of loose efflorescence. First, the specimens were longitudinally cut into two halves. Afterwards, these halves were split by progressively disaggregating them on sandpaper. Hence, salt distribution could be evaluated along two perpendicular directions.

The salt content in these samples was measured by means of the hygroscopic moisture content (HMC) method (Lubelli et al. 2004; Gonçalves and Rodrigues 2006; Gonçalves et al. 2006). After oven-drying at 40°C, the samples were kept inside a climatic chamber set-pointed at 20°C and 95% RH until hygroscopic equilibrium was achieved, that is, until their mass remained constant over time. A FITOCLIMA 500 EDTU® climatic chamber by Aralab (Portugal) was used.

Ten control-samples of only NaCl were simultaneously tested, as well as two non-contaminated samples of each base-material (mortar and stones). Since the HMC varies linearly with the salt content, it was possible to calculate the sample's actual salt content by considering the HMC of the base-materials (salt content = 0%) and of the control-samples (salt content = 100%).

Scope and precision of the HMC method were thoroughly discussed in a previous article (Gonçalves and Rodrigues 2006). As argued in it, minor variations of the environmental conditions (in particular of RH which, additionally, is much less homogeneous and stable in climatic chambers than temperature) may result in relevant variations of salt-solutions' equilibrium concentration. That uncertainty was evaluated by means of the ten NaCl control-samples which were distributed throughout the chamber. Average, minimum and maximum HMC of respectively 732%, 688% and 756% were obtained for those samples. Accordingly, the possible deviation of the salt content in the samples from the values in Fig. 13, which were calculated by means of the average HMC of the pure-salt samples, is of +6.4% or <minus>3.2% (as a percentage of the values in Fig. 13). This means that the climatic conditions in the chamber were quite homogenous.

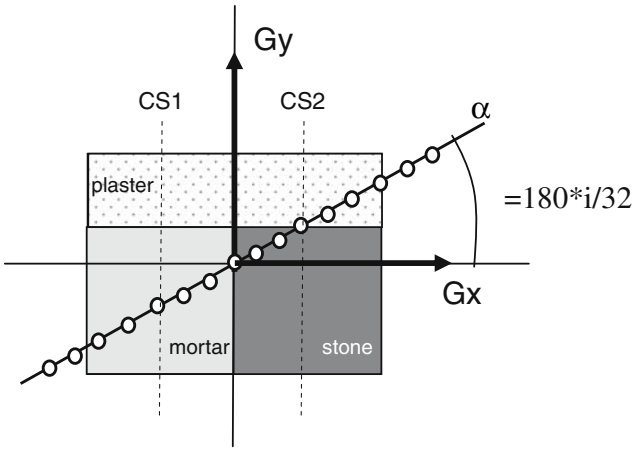

Fig. 4 Representation of 2D measurement on a sample. Using variable G_x and G_y gradient, cross-sections can also be measured in various directions. Using a backwards projection method out of these cross-sections, the moisture distribution can be calculated. Cross-sections CS1 and CS2 were measured in these experiments

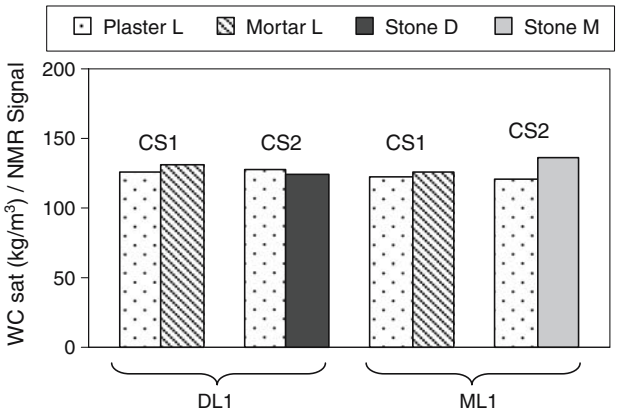

Fig. 5 Ratio moisture content/NMR signal at capillary saturation

Fig. 6 Colour scale for the MRI measurements (volumetric moisture content)

The average HMC of the pure-NaCl samples corresponds to an actual RH of 91.9% (at 20°C). That value was obtained by linear interpolation on NaCl water-activity (20°C)/molality tables (Robinson and Stokes 2002). As later confirmed the climatic chamber was actually working around 3% below the set-point of 95% RH. But this fact had no influence on the results because the sample's salt content was calculated by reference to the actual HMC of the salt and not by reference to thermodynamic data in the literature.

Results

Drying in the presence of pure water

Overall, the two specimens showed similar multi-stage drying behaviour. As can be seen in Figs. 7 and 8: (a) at first the surfaces remained wet; (b) after around 2 h the exposed surfaces began to dry faster; (c) the drying front receded into the material after 5 h in specimen DL1 and after 8 h in specimen ML1 (this is seen in Fig. 7, although from Fig. 8 suggests that complete drying of the surface occurs only at around 10 h in specimen DL1 and 14–18 h in specimen ML1).

In spite of this overall similarity, some important differences were also observed: (a) stone M contained a higher initial amount of moisture than stone D; (b) drying of stone M was faster than drying of stone D; (c) at the end of the experiments, stone M was clearly drier than stone D.

Drying in the presence of NaCl solution

NaCl did not modify the internal distribution of moisture throughout the drying process. This may be observed in Figs. 9 and 10 similar MRI image sequences were obtained for pure water and NaCl solution in either specimen. Still, these figures also show that when salt was present: (a) drying was much slower, as shown by the fact that the images correspond to later moments of drying in the case of NaCl; (b) no receding drying front was observed, in contrast to what occured for pure water, until the end of either experiment.

Overall drying curves

Overall drying curves (Fig. 11) were obtained by adding, for each of the four experiments, all the NMR signal values obtained at each moment at the two cross-sections (CS1 and CS2).

Evaporation from free liquid surfaces

Evaporation from free surfaces of pure water and NaCl saturated solution is reported in Fig. 12. In this figure it is seen that: (a) as expected, the evaporation rate from pure water is higher than from the salt solution in both environmental conditions; (b) the faster the evaporation, the lower the ratio between the drying rates of the two liquids; (c) however, in neither of the environmental conditions is the evaporation rate of pure water higher than twice the evaporation rate from the NaCl solution.

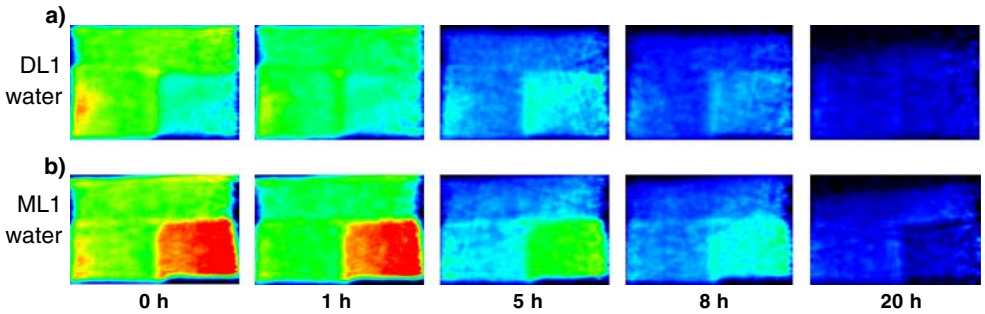

Fig. 7 Drying with pure water: MRI snapshots of specimens DL1 (**a**) and ML1 (**b**) in side-view. The receding drying front is identified when a dry (*dark*) surface layer exists on the top of the specimen. It is seen that it develops first in specimen DL1 and somewhat later in specimen ML1 (see supplementary material 2, 3)

Salt deposition

The final salt distribution in specimens DL1 and ML1 is shown in Fig. 14. It can be seen that in both specimens: (a) a higher concentration of salt occurred in the outer layer of the plaster; (b) a certain amount of salt is dispersed throughout the entire specimen.

In spite of these common features, relevant differences were also observed between the two salt distributions: (a) concentration of salt in the surface layer is higher for specimen ML1; (b) stone M accumulated less salt than stone D; (c) in specimen DL1 the salt accumulation peak occurred in stone D next to the plaster; (d) but in specimen ML1 the salt accumulation peak occurred in the bedding mortar next to stone M.

Discussion

Influence of NaCl on drying

Drying of homogenous porous materials has two main stages (Sherwood 1929; Scherer 1990): (a) during stage I liquid water is transported towards the surface, where it evaporates; (b) stage II starts when the unsaturated capillary flow is no longer able to supply water at a rate high enough to compensate surface evaporation and, thus, the drying front recedes into the specimen.

For pure water, specimens DL1 and ML1 clearly went through these two stages, despite their non-homogenous composition (Figs. 7, 8). Initially, during stage I, the moisture content decreased homogeneously. After around 2 h, the surfaces started drying faster. This is a transition period in which a decreasingly significant part of the porosity is involved in transporting liquid to the surface (for example: Scherer 1990; Rousset-Tournier 2001). During stage II the receding drying front first developed at around 5 h in specimen DL1 and 8 h in specimen ML1.

In the case of NaCl, the internal distribution of moisture during drying was similar to the case of pure water (Figs. 9, 10). However, because evaporation was slower, the liquid inside the specimens had more time to flow towards the evaporating surface. As a consequence, stage I was longer: no receding drying front developed until the end of the experiment when NaCl was present (60 h for specimen DL1 and 35 h for specimen ML1).

These results agree with: (a) theoretical considerations of Hall and Hoff (2002); (b) conclusions drawn from drying experiments performed on pure-water filled materials under distinct environmental conditions and monitored by means of gravimetric techniques, namely the recent experiments of Rousset-Tournier (2001) that showed that slower evaporation leads to a longer drying stage I and to the elimination of a higher amount of moisture during stage I; (c) previous 1D NMR measurements made at TUE in which slower drying and no receding drying front were observed in NaCl-contaminated materials (Pel et al. 2003; Petković 2005).

In real walls, slower evaporation also causes the increase of capillary rise. Therefore, the results obtained are also consistent with many practical observations that larger moist areas are recurrently found in salt-loaded masonry (for example: Massari and Massari 1993; Burkinshaw and Parret 2004).

For pure water, the drying rate is expected to be constant during stage I. This was observed in the present experiments: for pure water, the overall NMR drying curves (Fig. 11) resemble ordinary gravimetric drying curves even though the tested specimens are not homogeneous. But for NaCl, stage I drying rate decreased over time in both specimens.

Three main factors have been identified as possible causes of the lower and decreasing drying rate of salt-

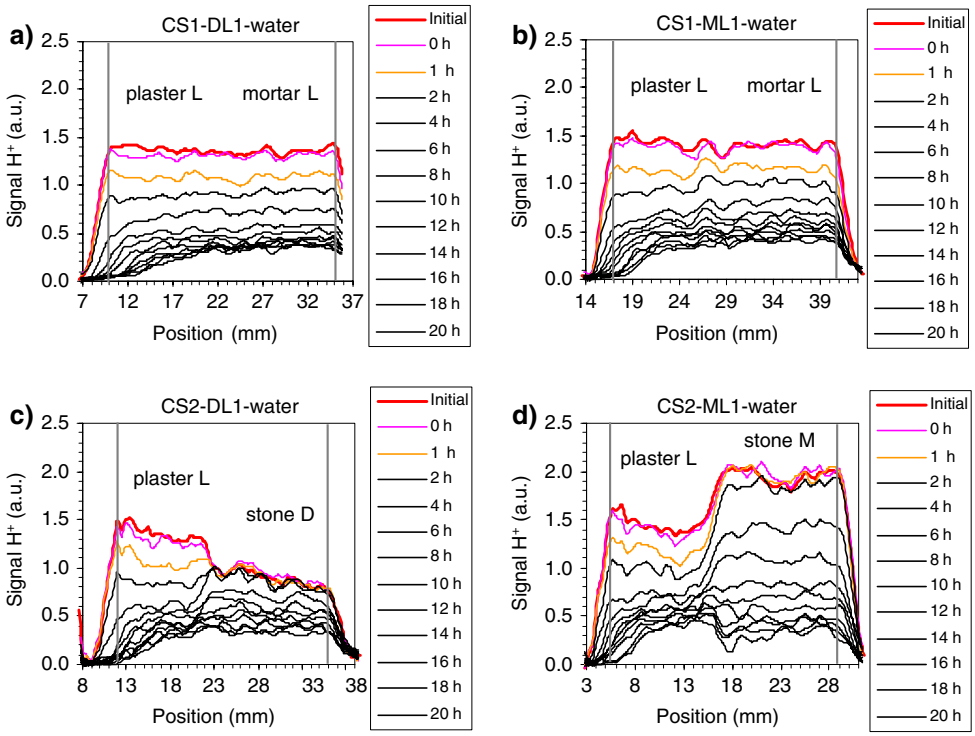

Fig. 8 Drying with pure water: 1D moisture profiles at cross-sections CS1 and CS2 of specimens DL1 and ML1 (position of the two cross-sections is indicated in Fig. 3). NMR signal is given in arbitrary units (*a.u.*). The *grey vertical line*-segments represent the physical limits of the test-specimens (in each chart, the drying surface corresponds to the segment on the *left*)

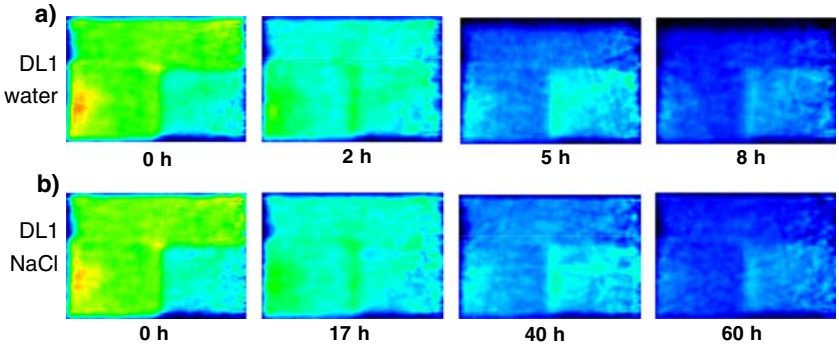

Fig. 9 MRI snapshots of specimen DL1 (*side-view*) during drying with: **a** pure water; **b** 3 m NaCl solution. The receding drying front is already visible after 5 h in specimen DL1 (the *dark area on the top* of the specimen corresponds to the dry surface layer). Notice that similar MRI images correspond to distinct moments of the drying in either specimens (see supplemetary material 4)

contaminated materials during stage I (Hall and Hoff 2002; Huinink and Pel 2003): (a) the RHeq of salt solutions is lower than that of pure water, thus, the driving RH gradient for vapour transport between the surface and the environment is also lower; (b) as evaporation proceeds, solutions become more and more concentrated at the drying front, hence, their RHeq decreases further; (c) once saturation is attained, the deposition of salt crystals may hinder evaporation.

Our results suggest that the low drying rates observed for the NaCl-contaminated specimens are mainly due to the reduction of a specific surface of evaporation, possibly caused by deposition of salt crystals with a blocking effect. As shown in Fig. 12, the faster the evaporation, the closer the evaporation rates of pure water and of the saturated NaCl solution. However, even for the faster drying conditions (20°C-15% RH), the ratio is only 1.4. The MRI-monitored drying experiments were performed under environmental conditions (18°C-0% RH) that are expected to generate faster evaporation than either of these and, thus, also an even lower ratio between the evaporation rates of the two liquids. In spite of that, in the MRI

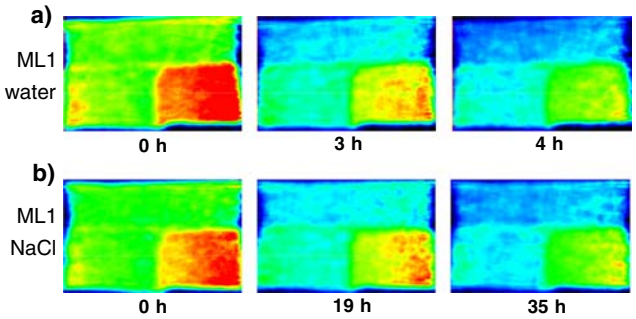

Fig. 10 MRI snapshots of specimen ML1 (*side-view*) during drying with: **a** pure water; **b** 3 m NaCl solution. Notice that similar MRI images correspond to distinct moments of the drying in the two specimens (see supplementary material 5)

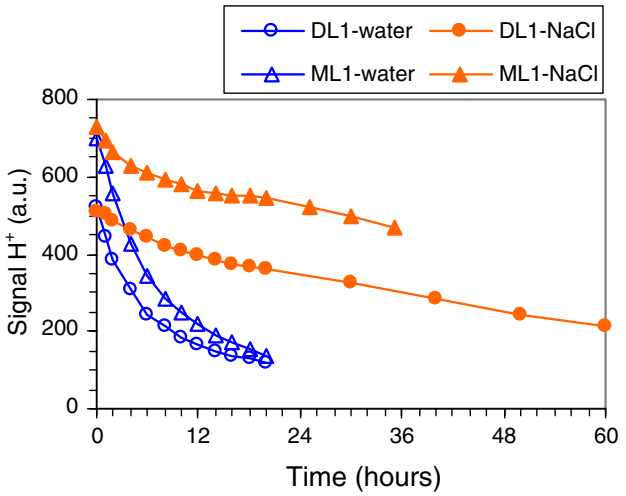

Fig. 11 Overall drying curves

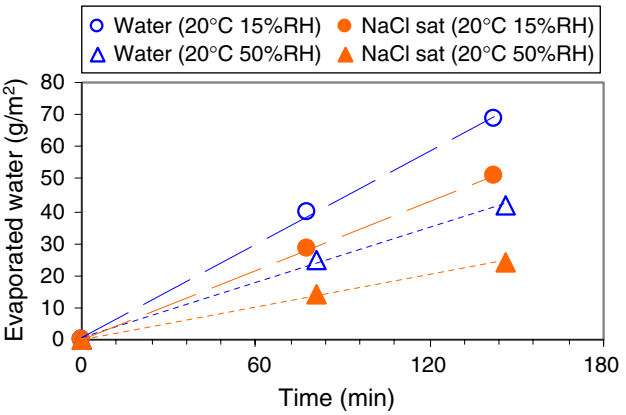

Fig. 12 Evaporation of pure water and saturated NaCl solution from free surfaces

experiments, the stage I drying rate was at least six times (specimen DL1) and three times (specimen ML1) higher for pure water than for the NaCl solution (Fig. 11). Therefore, it is clear that some factor other than the lower RHeq of the salt solution made a major contribution towards lowering evaporation.

Salt distribution

Salt distribution was evaluated from direct measurements of the salt content in distinct layers of the specimens (Fig. 13). Overall similarities were observed between the two specimens:

(a) A higher concentration of salt occurred always at the outer layer of the plaster clearly because the moisture was eliminated mostly by (stage I) surface evaporation.

(b) The second most superficial layer of plaster also presented always high salt content. This probably means that the drying front progressed inwards the specimens during the final oven-drying at 40°C.

(c) The deposition of a certain residual amount of salt throughout the whole specimen can be explained by the decrease in the moisture content at the pore level (Rose 1963). Critical moisture content is attained at a certain moment, at which liquid continuity is interrupted in the capillaries. Isolated clusters of liquid remain thus dispersed in the porous system, trapped in the finer pores. Further drying occurs by local evaporation, hence, in the case of a salt solution, a certain amount of salt will crystallize at each cluster.

Nevertheless, the final salt distribution is not completely identical for the two specimens. We attribute this to the different properties of stone D and stone M. That suggest that, when the masonry stone is varied, the local salt distribution may differ. This conclusion agrees with previous 1D drying experiments on plaster substrate specimens. It was found that a fine-pored plaster applied over coarse-pored substrate leads to crystallization only at the surface of the plaster, while a coarse-pored plaster applied over a fine-pored substrate induces crystallization both at the surface and at the interface plaster/substrate (Petković 2005). In our case, the main differences identified were the following:

1. The concentration of salt in the plaster, especially in the surface layer, is higher for specimen ML1. This is attributed to the fact that specimen ML1 contained a higher initial amount of salt solution.
2. Stone M, despite its higher initial solution content, accumulated less salt than stone D. This occurred probably because a pore can only remove water from another pore if it has higher capillary pressure, that is, if it is smaller. Stone M has a larger amount of big pores than stone D (Fig. 2). Thus,

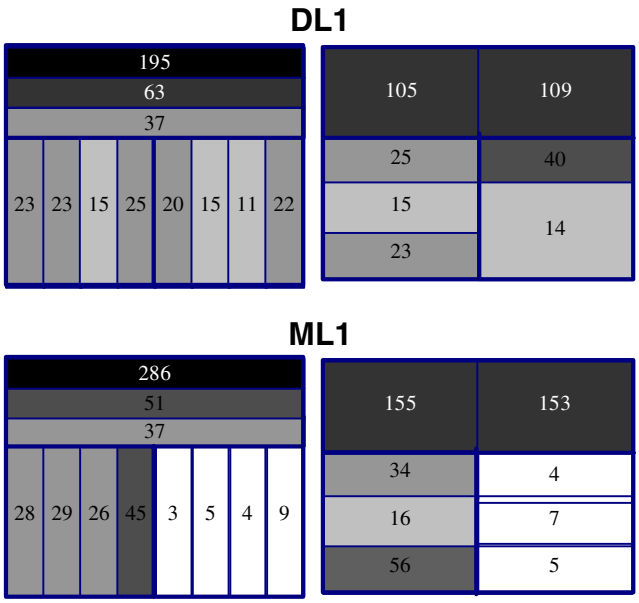

Fig. 13 Final salt distribution in specimens DL1 and ML1 (kg NaCl/m^3 open porosity in the stone). Both halves of either specimen are in side-view (Fig. 4)

mortar L is able to drain stone M faster and more completely. This behaviour was observed in the drying experiments with pure water (Fig. 8).

3. In the bedding mortar, a particularly high concentration of salt exists in the contact layer with stone M (Fig. 13c). This is most likely due to the following facts: stone M dries before the bedding mortar dries (Fig. 7); hence, when the stone is already dry, the mortar still contains enough moisture to ensure liquid continuity in the capillaries; hence, a transverse drying front develops at the mortar/stone interface and some salt accumulates in the first contiguous mortar layer.
4. In stone D, a higher accumulation of salt occurred close to where it came into contact with the plaster (Fig. 13b). This is probably due to the fact that the critical moisture content of porous materials is higher for less homogeneous pore size distributions (Snethlage and Wendler 1997). This is the case with mortar L when compared with the two stones (Fig. 2). Thus, although the results of drying with pure water (Fig. 8c) suggest that stone D is slightly dryer at the end of the experiment, liquid continuity may have been interrupted first in the plaster. In this case, a drying front develops at the plaster/stone interface. However, the MRI drying experiments ended before that could be observed. Therefore, further confirmation is needed. This effect is not so clear in the horizontal direction (Fig. 13a) probably because, due to the hindering effect of the interface, the plaster dries somewhat faster than the bedding mortar.

Other soluble salts

Only NaCl was studied here. Other salts may have different RHeq and crystallization properties and so distinct influences on drying. This may explain why some salts tend to form efflorescence while others are deposited deeper inside porous materials.

The evaporation rate condition also the rise of moisture in walls and, thus, the height at which salt crystals are deposited (Arnold 1989). For example, external factors such as a high environmental RH, low air velocity or the presence of impermeable coverings hinder surface evaporation and, hence, increase the height of capillary rise and salt deposition in walls. However, as seen, the salts themselves influence evaporation. Further work is needed to understand what exactly the influencing factors are. Nevertheless, it seems clear that some properties of the salts and perhaps of their crystallization process that influence drying need also to be considered in order to understand why some salts tend to crystallize higher on walls, while others tend to be deposited closer to the pavement.

It is probable that the concentration of salt solutions is, in certain cases, relevant. Concentration determines the RHeq of salt solutions. It may also condition the rate of crystallization in porous materials. Therefore, it may influence drying of masonry although the possible relevance of this influence requires further evaluation. Nevertheless, it is reasonable to expect that the lower the concentration, the more similar to the case of pure water is the drying process that is, the deeper in walls the drying front is positioned. This would explain why very weak salt solutions are able to cause significant damage in ancient constructions.

NaCl did not seem to significantly affect the interaction between the different materials during drying (Figs. 9, 10). Although the duration of the experiments with NaCl was insufficient for a complete comparison of the two drying processes, the measured salt distributions are compatible with this hypothesis, as discussed in the previous section. It is necessary to verify, in future work, if the same happens with other soluble salts. Different interaction between the various masonry materials during drying may lead to distinct local salt distribution patterns.

Acknowledgments MRI drying experiments were performed at the Centre for Material Research with Magnetic Resonance of Eindhoven University of Technology (TUE). The remaining

work was done at the National Laboratory of Civil Engineering (LNEC), in Lisbon. We are thankful to LNEC for sponsoring the two stays of T. Diaz Gonçalves at TUE and the Calouste Gulbenkian Foundation in Lisbon for co-sponsoring the first of these stays. We are indebted to Henk Huinink for his continued cooperation and for the useful discussions we had. Thanks to Kristina Terheiden for helping reviewing this paper. We are also grateful to the referee of this paper for his/her quick answer and useful comments, particularly for drawing our attention to the need of discussing the influence of the boundary conditions in the HMC measurements. We also thank LNEC technicians João Júnior, who made the specimens, and Luís Nunes, who carried out the MIP measurements. We are also thankful to Angela O'Driscoll for the valuable editorial suggestions.

References

Arnold A (1989) Salt weathering on monuments. Paper presented at the 1st international symposium on the conservation of monuments in the Mediterranean basin, Bari

Burkinshaw R, Parret M (2004) Diagnosing damp. RICS, Coventry, UK. ISBN 1-84219-097-0

Gonçalves TD, Rodrigues JD (2006) Evaluating the salt content of salt-contaminated samples on the basis of their hygroscopic behaviour. Part I: Fundamentals, scope and accuracy of the method. J Cult Herit 7:79–84

Gonçalves TD, Rodrigues JD, Marinho Abreu M (2006) Evaluating the salt content of salt-contaminated samples on the basis of their hygroscopic behaviour. Part II: experiments with nine common soluble salts. J Cult Herit 7:193–200

Gonçalves TD, Rodrigues JD (2005) Compatibility of rendering systems with salt-loaded ordinary masonry walls. Paper presented at the international RILEM workshop on repair mortars for historic masonry. Delft University of Technology, Faculty of Civil Engineering, The Netherlands, 26–28 January 2005

Hall C, Hoff WD (2002) Water transport in brick, stone and concrete. Spon Press, New York. ISBN 0-419-22890-X

Harris SY (2001) Building pathology. Deterioration, diagnostics, and intervention. Wiley, New York. ISBN 0-471-33172-4

Huinink HP, Pel L (2003) Modelling simultaneous drying and salt crystallization. End-report of the EC research project COMPASS, contract EVK4-CT-2001-0047–DG XII

Lubelli B, Van Hees RPJ, Brocken HJP (2004) Experimental research on hygroscopic behaviour of porous specimens contaminated with salts. Constr Build Mater 18:339–348

Massari G, Massari I (1993) Damp buildings – old and new. ICCROM, Rome. ISBN 92-9077-111-9

Pel L, Huinink H, Kopinga K (2003) Salt transport and crystallization in porous building materials. Magn Reson Imaging 21:317–320

Petrović J (2005) Moisture and ion transport in layered porous building materials: a Nuclear Magnetic Resonance study. PhD, Eindhoven University of Technology, The Netherlands. ISBN 90-386-2151-5

Robinson RA, Stokes RH (2002) Electrolyte solutions. Dover, New York. ISBN 0-486-42225-9. Second revised edition of the work originally published in 1959 by Butterworth, London

Rose DA (1963) Water movement in porous materials: Part 2—the separation of the components of water movement. Br J Appl Phys 14:491–496

Rousset-Tournier B (2001) Transferts par capillarité et évaporation dans des roches—Rôle des structures de porosité (Capillary moisture transfers and evaporation in stones—Role of porosity structures). PhD, University Louis Pasteur, Strasbourg, France

Scherer GW (1990) Theory of drying. J Am Ceram Soc 73:3–14

Sherwood TK (1929) the drying of solids II. Ind Eng Chem 21:976–980

Snethlage R, Wendler E (1997) Moisture cycles and sandstone degradation. In: Baer NS, Snethlage R (eds) Saving our architectural heritage: the conservation of historic stone structures. Elsevier, Chichester, UK

Steiger M, Behlen A, Newmann H-H, Willers U, Wittenburg C (1997) Sea salt in historic buildings: deposition, transport and accumulation. Paper presented at the 4th international symposium on the conservation of monuments in the Mediterranean basin, Rhodes 6–11 May 1997

Westbrook C (2002) MRI at a glance. Blackwell Science, Malden, USA. ISBN 0-632-05619-3